

# Full control of superconducting qubits with combined on-chip microwave and flux lines

Riccardo Manenti, Eyob A. Sete, Angela Q. Chen, Shobhan Kulshreshtha, Jen-Hao Yeh, Feyza Oruc, Andrew Bestwick, Mark Field, Keith Jackson, and Stefano Poletto  
*Rigetti Computing, 775 Heinz Avenue, Berkeley, CA 94710*

(Dated: July 14, 2021)

As the field of quantum computing progresses to larger-scale devices, multiplexing will be crucial to scale quantum processors. While multiplexed readout is common practice for superconducting devices, relatively little work has been reported about the combination of flux and microwave control lines. Here, we present a method to integrate a microwave line and a flux line into a single “XYZ line”. This combined control line allows us to perform fast single-qubit gates as well as to deliver flux signals to the qubits. The measured relaxation times of the qubits are comparable to state-of-art devices employing separate control lines. We benchmark the fidelity of single-qubit gates with randomized benchmarking, achieving a fidelity above 99.5%, and we demonstrate that XYZ lines can in principle be used to run parametric entangling gates.

Superconducting quantum processors are one of the leading platforms for near-term applications and large-scale quantum computing due to their flexibility in design, high-fidelity single- and two-qubit gates [1–4] and fast readout operations [5–7]. An architecture with a square grid of superconducting qubits for the implementation of the surface code requires each qubit to be coupled to four nearest neighbors as well as individual control lines and resonators [8, 9]. Routing the control lines on the perimeter of a monolithic device poses some challenges to scaling and several techniques have been developed to address this problem, including through-silicon vias and 3D coaxial architectures [10–12]. 3D wiring is not the only challenge for the development of a scalable architecture. As superconducting devices proceed past the 10-qubit era [8, 9, 13, 14], it becomes necessary to multiplex the waveguides on the chip. This is already a common practice for readout lines [15, 16] but little work has been reported on the combination of flux (Z) and microwave control (XY) lines because of the different nature of their coupling to the qubit. The combination of these lines into a single “XYZ line” would approximately halve the number of on-chip input and output ports for a quantum computer based on tunable qubits, thereby reducing the complexity of the design and the circuitry in general.

A technical challenge in combining flux and control lines on a planar geometry comes from the different natures of their coupling to the qubit. The Z line is designed to provide an inductive coupling to the SQUID loop that is high enough to bias the qubit at a specific frequency with a relatively small current such that the overall thermal dissipation does not lead to excessive heating. This can be done by shorting the Z line to ground approximately  $10\ \mu\text{m}$  away from the SQUID loop. The XY line instead is capacitively coupled to the qubit pads. To minimize the impact on the qubit relaxation time, the capacitive coupling to the  $50\ \Omega$  line cannot be too high [17]. At the same time, it cannot be too small otherwise strong microwave signals would be needed to operate single-qubit

gates. For silicon substrates with a relative permittivity at low temperature  $\epsilon_r = 11.45$  [18], these requirements are typically satisfied by positioning the end of the XY line at least  $50\ \mu\text{m}$  away from the nearest qubit pad. Hence, combining flux and control lines on the same plane of the qubits can be problematic because of these different interplays.

In this work, we propose and experimentally demonstrate one possible way to combine XY and Z lines into a single XYZ line. By moving the XYZ lines to the surface of the cap using a flip-chip approach [19], the medium separating the line from the qubit is vacuum whose relative permeability and permittivity are both one. This brings the capacitive and inductive coupling between the XYZ line and the qubit on an equal footing. We show empirical evidence that our approach meets the stringent requirements of qubit applications: keeping a high qubit coherence, supporting microwave drives, and delivering DC and RF flux pulses to the qubits.

The device used for this investigation includes four tunable qubits, each capacitively coupled to a readout resonator. The cap contains two separate readout lines (each capacitively coupled to two resonators) and four XYZ lines, one per qubit. Most of the cap surface is covered with a meshed ground plane. The region of the cap that surmounts the qubits and resonators is characterized by a  $24\ \mu\text{m}$  deep cavity [20]. The device is bonded to a  $6 \times 6\ \text{mm}^2$  cap with a flip-chip bonder that provides an alignment precision of a few micrometers. Since the height of the flattened indium bumps is about  $3\ \mu\text{m}$ , the distance between the qubit and the ground plane above is  $27\ \mu\text{m}$  (see Fig. 1 for an optical image of the qubit and the associated XYZ line on top). The electrical connection between the two chips is tested at room temperature with dedicated test structures. The cap is wirebonded to a printed circuit board and mounted to the coldest plate of a dilution refrigerator with a  $10\ \text{mK}$  base temperature.

The attenuation and filtering of the XY and Z fridge lines connecting the room temperature instrumentation to the device are different. This is because the XY lines

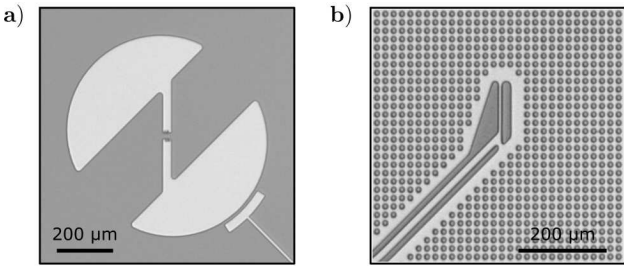


FIG. 1. **A qubit and its associated XYZ line.** **a)** Optical image of one qubit. The silicon substrate is in gray and the niobium film in lighter gray. The two superconducting pads are connected by a SQUID in the center of the image. **b)** Optical image of the corresponding XYZ line on the cap. Almost the entire surface is covered by a meshed ground plane.

must support microwave signals in the 3-7 GHz band, which is the typical qubit frequency band. In addition, these lines must have a strong attenuation to reduce the thermal noise reaching the device [21]. The Z lines instead provide low frequency pulses (DC – 1.5 GHz) in order to bias the qubits at specific sweet spots and operate parametric entangling gates [22]. The Z lines require a smaller attenuation than the XY lines.

Due to the different filtering requirements, the XY and Z fridge lines are combined at the lowest temperature plate of the dilution refrigerator. To this end, we have developed an in-house cryogenic diplexer as shown in Fig. 2a. This device allows us not only to combine low and high frequency signals but also to filter the frequency components outside a specific frequency band by using a network of inductors and capacitors. To mitigate the injection of quasi particles generated by high-frequency photons, the diplexer also includes an eccosorb filter on the output line [23, 24]. Figure 2b shows the measured transmission coefficient of a typical diplexer at room temperature and at 4 K. The diplexer was designed to have a 3-7 GHz bandpass filter for the XY line (port 1) and a 1.5 GHz low-pass filter for the Z line (port 2). The transmission coefficient from port 1 to port 2 (not shown in the figure) is lower than –20 dB up to 15 GHz. In our experiment, one diplexer per qubit is thermally anchored to the 10 mK stage of the dilution refrigerator. We have performed several cool downs and we have not noticed any degradation of their functionalities.

The geometry of the XYZ line has been engineered to obtain an upper limit on  $T_1$  greater than 200  $\mu$ s, a mutual inductance with the SQUID loop of approximately 500 nH and a capacitive coupling high enough to enable 20 ns  $\pi$ -pulses with our fridge setup (see Supplementary Information for a schematic of the fridge). To optimize these design parameters, we have performed full wave microwave simulations. The mutual inductance was tuned by varying the distance between the XYZ line and the SQUID as well as the width and length of the inductors

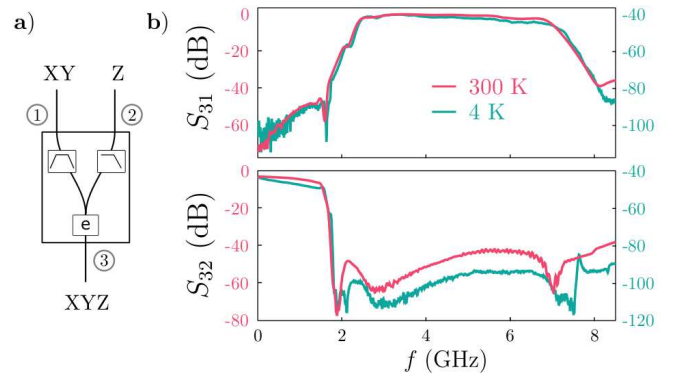


FIG. 2. **The diplexer.** **a)** Diagrammatic representation of the cryogenic diplexer. The input port 1 (2) receives 3-7 GHz (DC-1 GHz) microwave signals. They get combined and routed to port 3. The diplexer includes a low pass filter, a band pass filter and an eccosorb. **b)** Measured transmission coefficient between ports 1 → 3 and 2 → 3 for a typical diplexer at room temperature (magenta curve) and at 4 K (teal curve). The cryogenic measurements were taken with a 40 dB attenuation between the VNA and the diplexer inside the cryostat.

shorting the line to ground. The mutual inductance can also be adjusted by changing the area of the SQUID loop. However, its perimeter cannot be too long in order not to limit the qubit coherence [25]. With regards to the capacitive coupling, the area of the XYZ line that surrounds the qubit pads affects the coupling strength. As a result, the capacitive coupling can vary depending on the qubit geometry. The geometry illustrated in Fig. 1b is the result of an optimization process that takes into account the qubit relaxation time and the capacitive and inductive couplings.

Characterization of the device at base temperature shows that we can tune the qubit frequencies between 3.0 – 3.8 GHz. The median of the relaxation time for all of the qubits over a day is  $\tilde{T}_1 = 53 \mu$ s, and transverse relaxation times at the maximum qubit frequency is  $\tilde{T}_2^* = 10 \mu$ s and  $\tilde{T}_{2E} = 49 \mu$ s. The relaxation times fluctuate over time (see Supplementary Information). This phenomenon has been reported elsewhere [26, 27].

We first verify the functionality of the XY lines by testing their ability to manipulate the qubit state. After some initial Rabi experiments, we optimize 100 ns DRAG Gaussian pulses and measure a single-qubit gate fidelity of  $99.77 \pm 0.02\%$  with randomized benchmarking for qubit 1 (see the inset of Fig. 3a). The theoretical limit imposed by the relaxation time of this qubit is 99.84% [28]. This demonstrates that high-fidelity single-qubit gates can be implemented with the XYZ lines.

We first assess that the XYZ lines can be used to deliver flux signals to the qubits. We measure the qubit frequency  $f_q$  as a function of the applied DC current as shown in Fig. 3a. The qubit frequency is measured with spectroscopic measurements and Ramsey experiments.

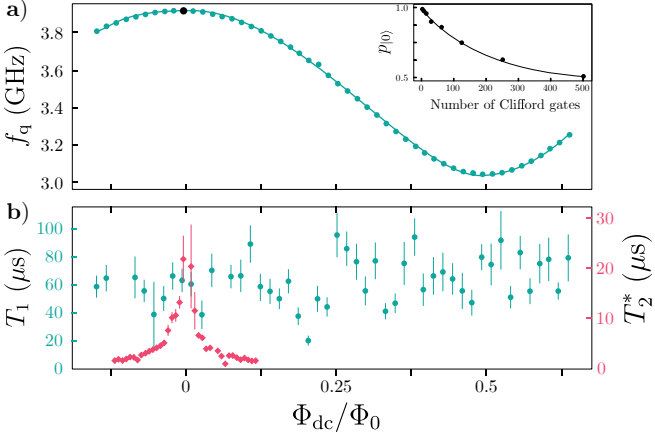


FIG. 3. **Characterization.** **a)** Qubit frequency as a function of flux bias. The black dot represents  $f_{\max}$ . Inset: randomized benchmarking with optimized 100 ns single-qubit gates run at  $f_{\max}$ . The solid line is a fit to  $A p^n + B$ . From the fit, we extract a single-qubit gate fidelity of  $99.77 \pm 0.02\%$ . **b)** Measured relaxation time  $T_1$  (teal dots) and transverse relaxation time  $T_2^*$  (magenta diamonds) as a function of flux bias. The error bars represent the uncertainty of the exponential fit for each experiment.

The data points are fitted with an analytical transmon model. At each flux bias, we measure the relaxation time  $T_1$  (see Fig. 3b). The value of  $T_1$  does not show a significant flux dependence and its average value is  $75 \mu\text{s}$ . Figure 3b includes the measurement of  $T_2^*$  as a function of flux close to the DC sweet spot. As expected, the transverse relaxation time increases substantially at the sweet spot where the sensitivity of the qubit frequency to flux noise is the lowest. Close to the DC sweet spots,  $T_2^*$  is above  $10 \mu\text{s}$  allowing high-fidelity single-qubit gates. Other devices fabricated on the same wafer show similar performance although they were measured without XYZ lines. We can thus conclude that XYZ lines can be used to tune the qubit frequency without compromising their relaxation time.

Next, we validate the ability of the XYZ lines to support RF flux pulses, crucial for the implementation of parametric entangling gates [22, 29]. In our experiment, the qubit starts at its maximum frequency  $f_{\max}$ . A flux RF pulse  $\Phi(t) = \Phi_{\text{dc}} + \Phi_{\text{ac}} \cos(\omega_d t)$  is delivered to the qubit where  $\Phi_{\text{dc}}$  is the DC bias,  $\Phi_{\text{ac}}$  is the flux pulse amplitude and  $\omega_d$  is the pulse frequency. The flux pulse induces periodic oscillations of the qubit frequency. The time average qubit frequency is measured with a Ramsey type experiment with the parametric modulation applied between two  $\pi/2$  pulses. Figure 4 shows the measured effective qubit frequency as a function of the flux pulse

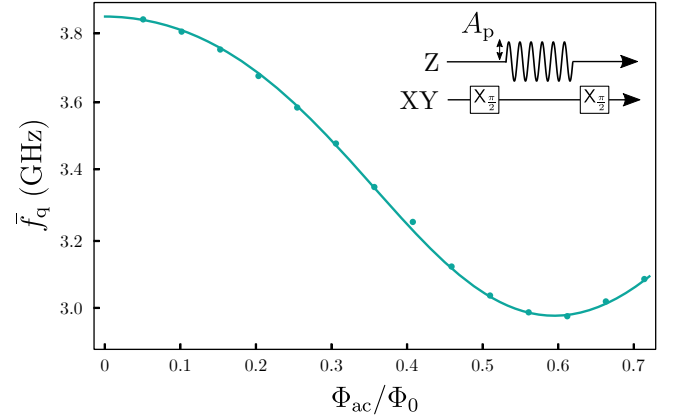


FIG. 4. **Ramsey experiment with flux pulses.** Time average qubit frequency as a function of flux pulse amplitude in a Ramsey type experiment. The qubit is initially parked at the maximum frequency  $f_{\max}$ . After the first  $\pi/2$  pulse, a flux pulse with amplitude  $A_p$  is applied to the qubit. This pulse makes the qubit frequency oscillate about  $f_{\max}$ . This changes the effective qubit frequency to  $\bar{f}_q$ . The solid curve is a fit to Eq. (1). The amplitude has been expressed in terms of flux quanta using  $\Phi_{\text{ac}} = \beta A_p$  where the factor  $\beta = 0.510 \Phi_0/V$  has been extracted from a fit.

amplitude. The data points are fitted to [30]

$$\begin{aligned} \bar{f}_q(\Phi_{\text{ac}}) &= \frac{1}{T} \int_0^T f_q(t') dt' \\ &= \sum_{n \geq 0}^{\infty} s_n \cos(2\pi n \Phi_{\text{dc}}) J_0(2\pi n \Phi_{\text{ac}}) \end{aligned} \quad (1)$$

where  $T$  is the oscillation period,  $J_0(x)$  is the Bessel function of the first kind, and the constants  $s_n$  only depend on the Josephson and charging energies  $E_{J1}$ ,  $E_{J2}$ , and  $E_C$  (their analytical expression is presented in the Supplementary Information). In our experiment,  $\Phi_{\text{dc}} = 0$  since the qubit is initially parked at  $f_{\max}$ . The flux pulse amplitude can be expressed in terms of the amplitude  $A_p$  generated by the room-temperature instrumentation as  $\Phi_{\text{ac}} = \beta A_p$  where  $\beta$  is a factor that can be extracted from the fit. As shown in the figure, we were able to reach the AC sweet spot,  $f_{\min}$ , where we operate parametric entangling gates [31]. Devices with XYZ lines are now used in our lab to run parametric entangling gates routinely.

The combination of the XY and Z fridge lines into a single line by means of a cryogenic diplexer may lead to an undesired effect. When a  $\pi$  pulse is sent through the XY fridge line to excite the qubit, it produces a current that flows through the termination of the XYZ line. This current can inadvertently modulate the qubit frequency. In our setup, a 100 ns  $\pi$  pulse is implemented with a room-temperature amplitude of  $V_p = 0.3 \text{ V}$ . The signal reaching the device creates a magnetic field through the SQUID of  $\Phi_{\text{ac}} = 1.6 \cdot 10^{-4} \Phi_0$  (here, we assumed that the

attenuation of the line is 85 dB at the qubit frequency and the mutual inductance between the XYZ line and the SQUID is  $M = 500 \text{ fH}$ ). This flux does not modulate the qubit frequency by an appreciable amount. Indeed, by approximating Eq. (1) close to  $f_{\max}$  up to second order in  $\Phi_{\text{ac}}$ , we obtain

$$\delta f = \bar{f}_q - f_{\max} = -\frac{\pi^2 E_{J1}/E_{J2}}{2h(1+E_{J1}/E_{J2})^2} \sqrt{8E_{J\Sigma}E_C} \left( \frac{\Phi_{\text{ac}}}{\Phi_0} \right)^2 \quad (2)$$

and using the parameters for qubit 0 ( $E_{J1}/h = 2140 \text{ MHz}$ ,  $E_{J2}/h = 9040 \text{ MHz}$ ,  $E_C/h = 182 \text{ MHz}$ ,  $E_{J\Sigma} = E_{J1} + E_{J2}$ ), we obtain a frequency shift of  $\delta f = -79 \text{ Hz}$ . This shift is below the qubit linewidth and cannot be detected with Ramsey experiments.

In conclusion, we demonstrated full control of superconducting qubits by combining XY and Z lines into a single XYZ line. We showed that XYZ lines patterned on the surface of the cap can be used to implement fast single qubit-gates and tune the qubit frequency with both DC and fast flux biases. We tested the performance of single-qubit gates with randomized benchmarking achieving a fidelity as high as  $99.93 \pm 0.04\%$ . Realization of combined XY and Z lines can reduce the number of on-chip input ports, an important requirement when scaling superconducting quantum processors. The natural next step is to combine the XY cables and the Z cables into a single cable to further reduce the complexity of the fridge built out for quantum processors with a large number of qubits. This can be accomplished by engineering frequency-dependent attenuators. More sophisticated techniques for the multiplexing of the cables would require optical links [32].

## ACKNOWLEDGMENTS

This material is based upon work supported by Rigetti Computing and the Defense Advanced Research Projects Agency (DARPA) under agreement No. HR00112090058.

## CONTRIBUTIONS

R.M. and S.P. developed the proposal. R.M., E.A.S., and S.P. acquired the data. R.M., E.A.S. performed the data analysis. R.M. simulated and designed the device and the cap. J.-H.Y. simulated and designed the diplexer. F.O., A.B., M.F. and K.J. were responsible for the development of an optimal cap fabrication. R.M. wrote the manuscript. E.A.S., A.C., S. K., and S.P. edited the manuscript. S.P. was the principal investigator of the effort.

---

- [1] S. Sheldon, L. S. Bishop, E. Magesan, S. Filipp, J. M. Chow, and J. M. Gambetta, Characterizing errors on qubit operations via iterative randomized benchmarking, *Physical Review A* **93**, 012301 (2016).
- [2] M. Rol, C. Bultink, T. O'Brien, S. De Jong, L. Theis, X. Fu, F. Luthi, R. Vermeulen, J. de Sterke, A. Bruno, *et al.*, Restless tuneup of high-fidelity qubit gates, *Physical Review Applied* **7**, 041001 (2017).
- [3] Y. Sung, L. Ding, J. Braumüller, A. Vepsäläinen, B. Kanman, M. Kjaergaard, A. Greene, G. O. Samach, C. McNally, D. Kim, *et al.*, Realization of high-fidelity cz and zz-free iswap gates with a tunable coupler, *arXiv preprint arXiv:2011.01261* (2020).
- [4] S. S. Hong, A. T. Papageorge, P. Sivarajah, G. Crossman, N. Didier, A. M. Polloreno, E. A. Sete, S. W. Turkowski, M. P. da Silva, and B. R. Johnson, Demonstration of a parametrically activated entangling gate protected from flux noise, *Physical Review A* **101**, 012302 (2020).
- [5] E. Jeffrey, D. Sank, J. Mutus, T. White, J. Kelly, R. Barends, Y. Chen, Z. Chen, B. Chiaro, A. Dunsworth, *et al.*, Fast accurate state measurement with superconducting qubits, *Phys. Rev. Lett.* **112**, 190504 (2014).
- [6] T. Walter, P. Kurpiers, S. Gasparinetti, P. Magnard, A. Potočnik, Y. Salathé, M. Pechal, M. Mondal, M. Oppliger, C. Eichler, *et al.*, Rapid high-fidelity single-shot dispersive readout of superconducting qubits, *Physical Review Applied* **7**, 054020 (2017).
- [7] J. Heinsoo, C. K. Andersen, A. Remm, S. Krinner, T. Walter, Y. Salathé, S. Gasparinetti, J.-C. Besse, A. Potočnik, A. Wallraff, *et al.*, Rapid high-fidelity multiplexed readout of superconducting qubits, *Physical Review Applied* **10**, 034040 (2018).
- [8] F. Arute, K. Arya, R. Babbush, D. Bacon, J. C. Bardin, R. Barends, R. Biswas, S. Boixo, F. G. Brandao, D. A. Buell, *et al.*, Quantum supremacy using a programmable superconducting processor, *Nature* **574**, 505 (2019).
- [9] M. Gong, S. Wang, C. Zha, M.-C. Chen, H.-L. Huang, Y. Wu, Q. Zhu, Y. Zhao, S. Li, S. Guo, *et al.*, Quantum walks on a programmable two-dimensional 62-qubit superconducting processor, *arXiv preprint arXiv:2102.02573* (2021).
- [10] M. Vahidpour, W. O'Brien, J. T. Whyland, J. Angeles, J. Marshall, D. Scarabelli, G. Crossman, K. Yadav, Y. Mohan, C. Bui, *et al.*, Superconducting through-silicon vias for quantum integrated circuits, *arXiv preprint arXiv:1708.02226* (2017).
- [11] D.-R. W. Yost, M. E. Schwartz, J. Mallek, D. Rosenberg, C. Stull, J. L. Yoder, G. Calusine, M. Cook, R. Das, A. L. Day, *et al.*, Solid-state qubits integrated with superconducting through-silicon vias, *npj Quantum Information* **6**, 1 (2020).
- [12] J. Rahamim, T. Behrle, M. Peterer, A. Patterson, P. Spring, T. Tsunoda, R. Manenti, G. Tancredi, and P. Leek, Double-sided coaxial circuit qed with out-of-plane wiring, *Applied Physics Letters* **110**, 222602 (2017).
- [13] J. Otterbach, R. Manenti, N. Alidoust, A. Bestwick, M. Block, B. Bloom, S. Caldwell, N. Didier, E. S. Fried, S. Hong, *et al.*, Unsupervised machine learning on a hybrid quantum computer, *arXiv preprint arXiv:1712.05771* (2017).

[14] P. Jurcevic, A. Javadi-Abhari, L. S. Bishop, I. Lauer, D. F. Bogorin, M. Brink, L. Capelluto, O. Günlük, T. Itoko, N. Kanazawa, *et al.*, Demonstration of quantum volume 64 on a superconducting quantum computing system, arXiv preprint arXiv:2008.08571 (2020).

[15] M. Jerger, S. Poletto, P. Macha, U. Hübner, E. Il'ichev, and A. V. Ustinov, Frequency division multiplexing readout and simultaneous manipulation of an array of flux qubits, *Applied Physics Letters* **101**, 042604 (2012).

[16] J. Kelly, R. Barends, A. G. Fowler, A. Megrant, E. Jeffrey, T. C. White, D. Sank, J. Y. Mutus, B. Campbell, Y. Chen, *et al.*, State preservation by repetitive error detection in a superconducting quantum circuit, *Nature* **519**, 66 (2015).

[17] J. C. Bardin, D. H. Slichter, and D. J. Reilly, Microwaves in quantum computing, *IEEE Journal of Microwaves* **1**, 403 (2021).

[18] J. Krupka, J. Breeze, A. Centeno, N. Alford, T. Claussen, and L. Jensen, Measurements of permittivity, dielectric loss tangent, and resistivity of float-zone silicon at microwave frequencies, *IEEE Transactions on microwave theory and techniques* **54**, 3995 (2006).

[19] M. Vahidpour, W. O'Brien, J. T. Whyland, J. Angeles, J. Marshall, D. Scarabelli, G. Crossman, K. Yadav, Y. Mohan, C. Bui, V. Rawat, R. Renzas, N. Vodrahalli, A. Bestwick, and C. Rigetti, Superconducting through-silicon vias for quantum integrated circuits, [arXiv:1708.02226](https://arxiv.org/abs/1708.02226) (2017).

[20] W. O'Brien, M. Vahidpour, J. T. Whyland, J. Angeles, J. Marshall, D. Scarabelli, G. Crossman, K. Yadav, Y. Mohan, C. Bui, *et al.*, Superconducting caps for quantum integrated circuits, arXiv preprint arXiv:1708.02219 (2017).

[21] S. Krinner, S. Storz, P. Kurpiers, P. Magnard, J. Heimsoo, R. Keller, J. Luetolf, C. Eichler, and A. Wallraff, Engineering cryogenic setups for 100-qubit scale superconducting circuit systems, *EPJ Quantum Technology* **6**, 2 (2019).

[22] S. Caldwell, N. Didier, C. Ryan, E. Sete, A. Hudson, P. Karalekas, R. Manenti, M. da Silva, R. Sinclair, E. Acalá, *et al.*, Parametrically activated entangling gates using transmon qubits, *Physical Review Applied* **10**, 034050 (2018).

[23] A. D. Córcoles, J. M. Chow, J. M. Gambetta, C. Rigetti, J. R. Rozen, G. A. Keefe, M. Beth Rothwell, M. B. Ketchen, and M. Steffen, Protecting superconducting qubits from radiation, *Applied Physics Letters* **99**, 181906 (2011).

[24] R. Barends, J. Wenner, M. Lenander, Y. Chen, R. C. Bialczak, J. Kelly, E. Lucero, P. O'Malley, M. Mariantoni, D. Sank, *et al.*, Minimizing quasiparticle generation from stray infrared light in superconducting quantum circuits, *Applied Physics Letters* **99**, 113507 (2011).

[25] J. Braumüller, L. Ding, A. P. Vepsäläinen, Y. Sung, M. Kjaergaard, T. Menke, R. Winik, D. Kim, B. M. Niedzielski, A. Melville, *et al.*, Characterizing and optimizing qubit coherence based on squid geometry, *Physical Review Applied* **13**, 054079 (2020).

[26] J. J. Burnett, A. Bengtsson, M. Scigliuzzo, D. Niegce, M. Kudra, P. Delsing, and J. Bylander, Decoherence benchmarking of superconducting qubits, *npj Quantum Information* **5**, 1 (2019).

[27] S. Schlör, J. Lisenfeld, C. Müller, A. Bilmes, A. Schneider, D. P. Pappas, A. V. Ustinov, and M. Weides, Correlating decoherence in transmon qubits: Low frequency noise by single fluctuators, *Physical Rev. Lett.* **123**, 190502 (2019).

[28] S. Asaad, C. Dickel, N. K. Langford, S. Poletto, A. Bruno, M. A. Rol, D. Deurloo, and L. DiCarlo, Independent, extensible control of same-frequency superconducting qubits by selective broadcasting, *npj Quantum Information* **2**, 1 (2016).

[29] D. C. McKay, S. Filipp, A. Mezzacapo, E. Magesan, J. M. Chow, and J. M. Gambetta, Universal gate for fixed-frequency qubits via a tunable bus, *Physical Review Applied* **6**, 064007 (2016).

[30] N. Didier, E. A. Sete, M. P. da Silva, and C. Rigetti, Analytical modeling of parametrically modulated transmon qubits, *Physical Review A* **97**, 022330 (2018).

[31] N. Didier, E. A. Sete, J. Combes, and M. P. da Silva, ac flux sweet spots in parametrically modulated superconducting qubits, *Phys. Rev. Applied* **12**, 054015 (2019).

[32] F. Lecocq, F. Quinlan, K. Cicak, J. Aumentado, S. Didams, and J. Teufel, Control and readout of a superconducting qubit using a photonic link, *Nature* **591**, 575 (2021).

## SUPPLEMENTARY INFORMATION: XYZ LINES FOR SUPERCONDUCTING DEVICES

Riccardo Manenti, Eyob A. Sete, Angela Q. Chen, Shobhan Kulshreshtha, Jen-Hao Yeh, Feyza Oruc, Andrew Bestwick, Mark Field, Keith Jackson, Stefano Poletto.

*Rigetti Computing, Inc., Berkeley, CA*

### S1. Fridge setup and device parameters

The cables connecting the room temperature instrumentation to the device must be suitably filtered and attenuated. Figure S1a shows the fridge setup used in our work. The XY line has an overall attenuation of 66 dB at DC. The Z line has only one 20 dB attenuator installed at the 4 K plate. The diplexer shown at the bottom of the figure includes both microwave filters and eccosorb filters.

Table S1 reports the main device parameters. Here,  $f_r$  is the resonator frequency,  $f_q^{\max}$  ( $f_q^{\min}$ ) is the maximum (minimum) qubit frequency and  $\eta$  is the qubit anharmonicity. The coherence times  $\tilde{T}_1$ ,  $\tilde{T}_2^*$ , and  $\tilde{T}_{2E}$  are the median values measured at  $f_q^{\max}$ . It should be pointed out that these values fluctuate in the course of a day (See Fig. S2). This phenomenon is well-known in the community and has been investigated in Ref. [26, 27]). The figure of merit  $F_{1q}$  is the fidelity of 100 ns single-qubit gates measured with randomized benchmarking.

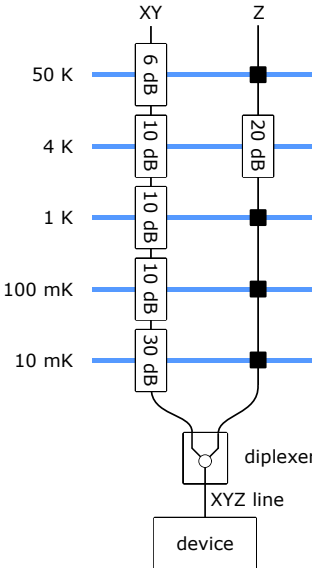


FIG. S1. **Fridge setup.** Diagram of the fridge setup. The black squares represent SMA connectors. These components ensure a good thermalisation of the coaxial cable.

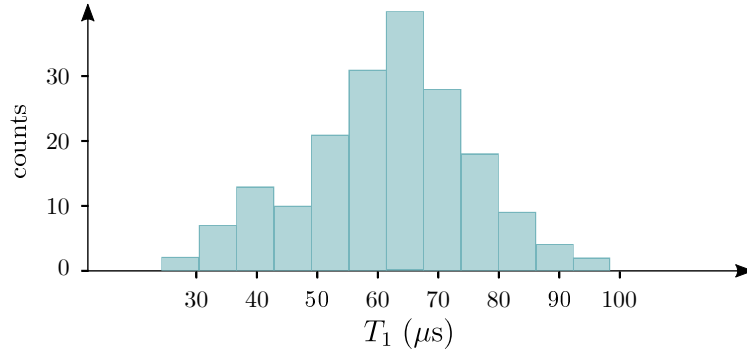


FIG. S2. **Repeated measurements of  $T_1$ .** Histogram of 60 measurements of the relaxation time of qubit 2 in the course of a day.

	q0	q1	q2	q3
$f_r$ (MHz)	7029	7122	7203	7292
$f_q^{\max}$ (MHz)	3851	3786	3919	3870
$f_q^{\min}$ (MHz)	2981	2956	3050	2936
$\eta$ (MHz)	-206	-208	-208	-210
$E_C$ (MHz)	182	185	185	186
$E_{J1}$ (MHz)	2140	2360	2160	2250
$E_{J2}$ (MHz)	9040	9090	9300	8860
$\tilde{T}_1$ (μs)	51	21	61	56
$\tilde{T}_2^*$ (μs)	10	16	10	1
$\tilde{T}_{2E}$ (μs)	81	25	60	31
$F_{1q}$ (%)	99.93	99.77	99.88	98.09

TABLE S1. Main parameters of the 4-qubit device investigated in this study.

## S2. Spurious qubit frequency modulation

Since in our fridge configuration the XY fridge line and the Z fridge line are combined together with a cryogenic diplexer, a control pulse at the qubit frequency sent through the XY fridge line can inadvertently modulate the qubit frequency. Let us assume that a  $\pi$  pulse has a room temperature voltage of  $V(t) = A_p \cos(\omega_d t)$ . This pulse generates a current through the on-chip XYZ line of

$$I(t) = 2\alpha \frac{V(t)}{R}, \quad \alpha = 10^{-\gamma/20} \text{ dB},$$

where  $\gamma$  is the attenuation of the line at the qubit frequency (in our case,  $\gamma \approx 85$  dB), and  $R = 50 \Omega$  is the impedance of the line. The factor of two takes into account the fact that the line is shorted to ground. The current produces a magnetic flux through the SQUID of

$$\Phi(t) = MI(t) = M2\alpha \frac{V(t)}{R},$$

where  $M$  is the mutual inductance between the line and the SQUID (for our device,  $M \approx 500$  fH). In our device, the amplitude required to implement a  $\pi$  pulse is  $A_p = 0.3$  V for a 100 ns pulse. Thus, the magnetic flux threading the SQUID is

$$\Phi(t) = M2\alpha \frac{A_p}{R} \cos(\omega_d t) = \Phi_{\text{ac}} \cos(\omega_d t), \quad \text{where} \quad \Phi_{\text{ac}} = 1.6 \cdot 10^{-4} \Phi_0.$$

Using Eq. (2) of the main text and the parameters for qubit 0, we conclude that the qubit frequency would shift by 79 Hz. This shift is well below the qubit linewidth and cannot be detected with Ramsey experiments.

### S3. Ramsey experiments with flux pulses

In this Section, we present the fitting function of the effective qubit frequency for the Ramsey experiment including flux pulses (Eq. (1) of the main text). Since the detailed derivation can be found in Ref. [30], we limit ourselves to report the final result. First, let us define the vector

$$\mathbf{c} = \left\{ 4, -1, -\frac{1}{2^2}, -\frac{21}{2^7}, -\frac{19}{2^7}, -\frac{5319}{2^{15}}, -\frac{6649}{2^{15}}, -\frac{1180581}{2^{22}}, -\frac{446287}{2^{20}} \right\},$$

and the constants

$$\xi = \sqrt{\frac{2E_C}{\sqrt{E_{J1}^2 + E_{J2}^2}}}, \quad \tilde{E}_J = \frac{2E_{J1}E_{J2}}{E_{J1}^2 + E_{J2}^2}.$$

We also need to introduce some coefficients  $s_n$ . For  $n = 0$ , we have

$$s_0 = E_C \sum_j c_j \xi^{j-2} {}_2F_1\left[\frac{j-2}{8}, \frac{j-2}{8} + \frac{1}{2}, 1, \tilde{E}_j^2\right],$$

where  ${}_2F_1(a, b, c, d)$  is the hypergeometric function. For  $n > 1$ , we have

$$s_n = \frac{2}{n!} E_C (-\tilde{E}_J/2)^n \sum_j c_j \xi^{j-2} \frac{\Gamma(n + \frac{j-2}{4})}{\Gamma(\frac{j-2}{4})} {}_2F_1\left[\frac{n}{2} + \frac{j-2}{8}, \frac{n+1}{2} + \frac{j-2}{8}, n+1, \tilde{E}_j^2\right],$$

where  $\Gamma(z)$  is the Euler gamma function. The effective qubit frequency is given by

$$\bar{f}_q(\Phi_{AC}) = \sum_{n=0}^p s_n \cos(2\pi n \Phi_{dc}) J_0(2\pi n \Phi_{ac}),$$

where  $p$  defines the accuracy of the perturbation.